Published in final edited form as:
NMR Biomed. 2013 November ; 26(11): 1547–1554. doi:10.1002/nbm.2989.

Resonant Inductive Decoupling (RID) for Transceiver Arrays to Compensate for both Reactive and Resistive Components of the Mutual Impedance

Nikolai I. Avdievich, **Jullie W. Pan**, and **Hoby P. Hetherington**
Department of Neurosurgery, Yale University, New Haven, CT 06520

Abstract

Transceiver surface coil arrays improve transmit performance ($B_1/\sqrt{kW}$) and B_1 homogeneity for head imaging up to 9.4 T. To further improve reception performance and parallel imaging the number of array elements has to be increased with correspondent decrease of their size. With a large number of small interacting antennas decoupling is one of the most challenging aspects in the design and construction of transceiver arrays. Previously described decoupling techniques using geometric overlap, inductive or capacitive decoupling have focused on eliminating only the reactance of the mutual impedance, which can limit the obtainable decoupling to −10 dB due to residual mutual resistance. A novel resonant inductive decoupling (RID) method, which allows compensation for both reactive and resistive components of the mutual impedance between the adjacent surface coils, has been developed and experimentally verified. This method provides an easy way to adjust the decoupling remotely by changing the resonance frequency of the RID circuit through adjustment of a variable capacitor. As an example a single row (1×16) 7T transceiver head array of n=16 small overlapped surface coils using RID decoupling between adjacent coils was built. In combination with overlapped coils the RID technique achieved better than −24 dB of decoupling for all adjacent coils.

Keywords

RF head coil; Transceiver arrays; array decoupling; high field MRI; mutual resistance

INTRODUCTION

At high magnetic field strengths where the object size becomes comparable to the RF wave length (e.g. body imaging at 3 T and above, head imaging at 7 T and above) increased RF inhomogeneity, decreased transmit efficiency (μT/√W) and increasing local specific absorption rate (SAR) pose significant limitations for conventional single-channel transmit volume coils. To overcome these limitations substantial effort has been focused on the development of transceiver phased arrays consisting of multiple independent (i.e. decoupled) RF antennas used simultaneously for both transmission and reception. Transceiver arrays provide improved homogeneity, enhanced transmit efficiency and decreased SAR through the use of RF shimming (1–5) and parallel transmission (6–8). Head arrays with surface coils as individual elements have been successfully utilized at 7 T (4,9,10) and above (11). In the surface coil array, loops of the RF current are normally positioned parallel to the surface of the array holder which circumscribes the head as opposed to stripline designs (1,12,13) where the current flows in a plane perpendicular to the

*Correspondence to: Nikolai I. Avdievich, Ph.D., Department of Neurosurgery, Yale University, MRRC/TAC, 300 Cedar St., New Haven, CT 06520. Telephone: (203) 785-6016. Fax: (203) 785-6643. nikolai.avdievich@gmail.com.

surface of the head. This orientation of antennas minimizes the mutual inductive coupling between the array's elements and simplifies decoupling by largely limiting significant coupling to only adjacent elements (14). Since transceiver arrays can also be used as conventional phased arrays for reception, receive sensitivity can, in principle, also be maintained. However, to provide sufficient coverage of the entire object during transmission and high signal-to-noise ratio (SNR) comparable with multi-channel receive-only arrays, transceiver arrays should consist of smaller overlapped RF surface coils. With a large number of interacting RF antennas decoupling is one of the most challenging and critical aspects in designing and constructing transceiver arrays. The fact that the same array elements are used for both transmission and reception dictates that preamplifier decoupling (15), cannot be utilized.

Overlapping of adjacent surface coils is one of the most common inductive decoupling techniques (15–17) and enables larger and greater numbers of RF coils to be used for a given circumference of the array. Maintaining the size of the individual coils in the array is important to preserve the penetration depth for RF transmission. Adjacent overlapped surface coils under loading can generate substantial mutual resistance, R_{12} (15,18), and often cannot be decoupled using additional common capacitive (1,10,12,19) or inductive decoupling methods (4,9,11,15), which compensate only for the mutual reactance. The mutual resistance is produced due to common current paths between the coil pair within the sample. For example, for a pair of overlapped loaded surface coils the ratio of R_{12}/R, where R is the resistance of each surface coil, can measure from 0.2 to 0.4 (15,18). This corresponds to the residual coupling in the range of −14 to −8 dB.

Resonant inductive decoupling (RID) provides a way to compensate for both the reactive and the resistive components of the mutual impedance, Z_{12} (20). It also offers an easy way to adjust the decoupling, by changing the resonant frequency of the decoupling circuit through adjustment of a single variable capacitor. However, the placement and the geometry of these RID elements are critical since the RF field generated by the RID can significantly alter the RF field of the array.

In this work we describe a novel RID technique, which provides for decoupling of array elements as well as minimization of resistive coupling. We also demonstrate the importance of both the geometry and orientation of the resonant loops in the RID element with respect to each other and the array itself in optimizing decoupling performance. As a demonstration of the technique we built a densely-populated single row (1×16) transceiver head array of small overlapped surface coils and acquired images of the human head at 7T.

THEORY

In this work we developed a new technique, which improves decoupling of individual antennas in a transceiver array. The term "decoupling" is used to describe the process of eliminating a "crosstalk" or the energy transfer between two coupled antennas through the shared impedance Z_{12}. The efficiency of decoupling as applied to transmission is evaluated by measuring the transmission parameter, S_{12}, which is directly related to the Z_{12} value. In this sense the resistive and reactive component of the Z_{12} simply describe the amplitude and phase relationship of a signal propagating between ports of two coupled antennas. As applied to reception the mutual resistance measured between two coupled antennas is often related to their noise correlation (15,18). Evaluation of the noise correlation between two resonant coils additionally coupled to a third resonant decoupling circuit is more complicated than that just for a pair of coils. It requires thorough theoretical consideration and is beyond the scope of this work.

Figure 1 shows two resonant decoupling circuits inductively coupled to a pair of surface coils. In the presence of a sample the mutual impedance Z_{12} may contain a substantial resistive component R_{12} due to common current paths between the coil pair within the sample. Fig. 1A presents a "butterfly" ("figure eight") RID coil while Fig. 1B depicts a regular surface coil. The matrix for the Kirchhoff equations describing the "figure eight" RID coil is given by Eq. [1]

$$\begin{pmatrix} V_1 \\ 0 \\ V_2 \end{pmatrix} = \begin{pmatrix} Z_1 & j\omega_L M_0 & -j\omega_L M + R_{12} \\ j\omega_L M_0 & Z_0 & -j\omega_L M_0 \\ -j\omega_L M + R_{12} & -j\omega_L M_0 & Z_2 \end{pmatrix} \begin{pmatrix} I_1 \\ I_0 \\ I_2 \end{pmatrix}. \quad [1]$$

where Z_0, Z_1, and Z_2 are corresponding impedances of the RID circuit and the two surface coils, M_0 is the mutual inductance between the RID and each surface coil (for simplicity we assumed them to be equal), and ω_L is the resonance frequency of the surface coils. Solving for V_1 and V_2 we obtain

$$\begin{pmatrix} V_1 \\ V_2 \end{pmatrix} = \begin{pmatrix} Z_1 + \frac{\omega_L^2 M_0^2}{Z_0} & -j\omega_L M + R_{12} - \frac{\omega_L^2 M_0^2}{Z_0} \\ -j\omega_L M + R_{12} - \frac{\omega_L^2 M_0^2}{Z_0} & Z_2 + \frac{\omega_L^2 M_0^2}{Z_0} \end{pmatrix} \begin{pmatrix} I_1 \\ I_2 \end{pmatrix}. \quad [2]$$

Similarly, for the RID design shown in Fig. 1B we obtain

$$\begin{pmatrix} V_1 \\ V_2 \end{pmatrix} = \begin{pmatrix} Z_1 + \frac{\omega_L^2 M_0^2}{Z_0} & -j\omega_L M + R_{12} + \frac{\omega_L^2 M_0^2}{Z_0} \\ -j\omega_L M + R_{12} + \frac{\omega_L^2 M_0^2}{Z_0} & Z_2 + \frac{\omega_L^2 M_0^2}{Z_0} \end{pmatrix} \begin{pmatrix} I_1 \\ I_2 \end{pmatrix}. \quad [3]$$

Near the resonance, Z_0 can be approximated as $Z_0 \approx 2jL_0(\omega_L - \omega_0) + R_0 = 2jL_0\Delta\omega + R_0$, where ω_0 is the resonance frequency of the decoupling circuit and L_0 and R_0 are its inductance and resistance. For the off diagonal elements in Eq.[2] we obtain

$$-j\omega_L M + R_{12} - \frac{\omega_L^2 M_0^2}{Z_0} \approx -j\omega_L L(k - \frac{k_0^2}{2\xi}) + R_{12} - \frac{R}{4}\frac{k_0^2}{\xi^2}\frac{Q}{Q_0}, \quad [4]$$

where $\xi = \Delta\omega/\omega_L$, R and L are the resistance and the inductance of the surface coils, and Q_0 and Q are corresponding Q-factors of the RID and the surface coils. We have also taken into account that $M_0 = k_0(LL_0)^{1/2}$, and $M = kL$, where k and k_0 are corresponding coupling coefficients. Again for simplicity we assume that R, L and Q are the same for both surface coils. From Eq.[4] when $\Delta\omega > 0$ ($\omega_0 < \omega_L$) both the real and the imaginary components of Z_{12} can be cancelled. To cancel the mutual reactance

$$k_0^2 = 2k\xi \quad [5]$$

Both the reactive and the resistive components of the Z_{12} are cancelled when

$$k_0 = k\sqrt{\frac{Q_0}{\eta Q}} \quad \text{and} \quad \xi = \frac{k}{2\eta}\frac{Q}{Q_0}, \quad [6]$$

where η is a ratio of R_{12}/R. Thus, by varying the coupling coefficient, k_0, and the frequency shift, ξ, both the real and the imaginary components of Z_{12} can be cancelled. Similarly, for the RID coil shown in Fig. 1B (Eq.[3]), the off diagonal elements are given by $-j\omega_L L(k + \frac{k_0^2}{2\xi}) + R_{12} + \frac{R}{4}\frac{k_0^2}{\xi^2}\frac{Q}{Q_0}$. Therefore, the reactive component of the Z_{12} can be cancelled when $\Delta\omega < 0$ ($\omega_0 > \omega_L$). However, this RID coil only adds to the R_{12} since both

resistive components have the same sign. The mutual inductance is eliminated when $k_0^2 = -2k\xi$. Thus this circuit also can be used for compensating the mutual reactance between two surface coils when $\xi<0$ ($\omega_0 > \omega_L$). However, ξ should be sufficiently large so as to not increase the resistive coupling. This can be achieved if the RID coil has larger coupling coefficient k_0 (e.g. larger loops). A major difference between two decoupling circuits shown in Figs.1A and B is that magnetic fluxes generated by surface coils #1 and #2 produce voltages of opposite sign in the "figure 8" RID coil (Fig.1A) versus producing voltages of the same sign in the RID circuit shown in Fig.1B. A situation similar to that shown in Fig.1A can be realized in a several different ways as shown, for example, in Figs. 2A–D. Decoupling circuits shown in Fig.2A (21) and Fig.2B (22) have been described previously. For all of these cases the Kirchhoff equations in Eq.[2] apply, such that these RID coils can decouple a pair of array elements when $\xi>0$ ($\omega_0<\omega_L$) as well as compensate for the resistive components of the Z_{12}. Figures 2E and 2F present two additional examples of RID circuits similar to that shown in Fig.1B and described by Eq. [3]. Again, these RID circuits cancel the mutual inductive coupling when $\xi<0$ ($\omega_0>\omega_L$) but cannot compensate for the resistive component of the Z_{12}. The design similar to that shown in Fig. 2F has also been previously described (23).

It is also of importance to evaluate the current I_0 flowing in the RID circuit. For example, for the "figure eight" RID from Eqs.[1] and [5] we obtain

$$I_0 = \frac{j\omega_L M_0}{Z_0}(I_2 - I_1) \approx \frac{k_0}{2\xi}\sqrt{\frac{L}{L_0}}(I_2 - I_1) = \frac{k}{k_0}\sqrt{\frac{L}{L_0}}(I_2 - I_1). \quad [7]$$

In the case of equal current amplitudes (i.e. $I_1=I_2=I$) the amplitude of $I_0 \approx \frac{k}{k_0}\sqrt{\frac{L}{L_0}} I \mathrm{Sin}\varphi$, where φ is the phase shift between I_1 and I_2.

EXPERIMENTAL

To demonstrate these concepts we built several 298 MHz (^{1}H frequency at 7T) 2-coil arrays with resonant (RID) and conventional non-resonant inductive decoupling for comparison. All of these arrays were built using non-overlapped rectangular surface coils of the same size (7.5 cm × 9 cm) with a 13 mm gap between adjacent (Δn=1) coils. Each surface coil was formed from copper tape (6.4 mm width) with six capacitors (100C series, American Technical Ceramics, Huntington Station, NY) uniformly distributed along the coil's length. All the coils were individually tuned and matched using variable capacitors (Voltronics, Denville, NJ). The RID coils (4 mm ID) were built using 18 gauge copper magnet wire (diameter 1 mm) and positioned at ~ 10 mm distance from the surface coil plane to increase the separation from the sample.

We also built a 16-coil single–row (1×16) array consisting of smaller (5.6 -width and 9 cm -length) overlapped rectangular surface coils (Fig.3). A schematic of an individual surface coil is shown in Fig.4. The surface coils were formed using 5 mm copper tape and overlapped by 12 mm. The coupling between adjacent coils (Δn=1), both reactive and resistive, was compensated by using the RIDs. RID circuits (3 mm ID) were constructed using 20 gauge (diameter 0.8 mm) magnet wire. The proximity of the next nearest surface coils (i.e. Δn=2) resulted in mutual inductive coupling of ~ 5 nH (k ~ 0.03). This coupling was eliminated by the use of conventional non-resonant inductive decoupling (4,9) as shown in Fig.4. For the non-resonant inductive decoupling circuits we used two-turn small (2.3 mm diameter) coils made of 20 gauge magnet wire and wound in opposite directions instead of single loop coils as described previously (4,9). To decrease radiation losses (24) a shield (50

μm polyamide film with a 5 μm copper layer, Sheldahl, Northfield, MN) was placed 4 cm away from the surface coils. To make sure that the RF field produced by RIDs is well localized and does not perturb the B_1 of the array within the head we measured transmit B_1 maps (phase and amplitude) (25). Then we compared them with the maps obtained with the same arrays but decoupled using conventional non-resonant inductive decoupling, which does not significantly perturb the RF field profile (4,9).

To mimic head loading conditions we constructed two phantoms both filled with NaCl and sucrose in water (26). The percentage by weight measured 41.7%, 56.3% and 2.1% for water, sucrose and NaCl, respectively. The conductivity and the dielectric permittivity measured 0.57 S/m and 52 respectively, which approximates that reported for the human head at 300 MHz (^{1}H resonance frequency at 7 T). The two-coil arrays were evaluated using a 2.0L spherical phantom (16 cm dia.). The 1×16 array was evaluated using a cylindrical phantom with an elliptical cross-section (14 cm × 17 cm). With the described solution this provides loading similar to that of an average sized human head. Coupling coefficients k and k_0 were estimated as previously described (27). Q-factors of RIDs were estimated from the frequency dependence of S_{12} and measured using a weakly coupled pair of pick up coils (28). Q-factors of the surface coils were evaluated using the frequency dependence of S_{11} (28). For the 1×16 array Q_U of individual surface coil elements measured 270. Q_L measured on an average size human head varied from ~ 70 (Q_U/Q_L = 3.9) for the posterior coils (closest to the head) up to ~100 (Q_U/Q_L = 2.7) for the anterior coils (furthest from the head).

All data were collected using a 7 Tesla Agilent system. To test the coil performance, gradient echo images (256 × 256 × 13 slices) from an adult subject and a phantom were collected using 2/8 mm slice thickness/gap, 19.2 cm × 19.2 cm field of view (FOV), TR = 400 ms, nominal flip angle 15°. B_1 maps of the individual coils (single coil transmitting) or the combined array (all coils transmitting simultaneously) were collected using a rapid gradient echo dual angle method (25) with 64 × 64 resolution, TR = 1 s, 5/5 mm slice thickness/gap centered on the matched gradient echo images. All human studies were performed under an IRB (Human Investigations Committee) approved development project.

RESULTS

First, the geometry of the RID circuit was optimized to insure that it did not perturb the profile of RF magnetic field B_1 produced by a pair of well decoupled surface coils. First, we evaluated the two RID geometries shown in Figs.2A (21) and 2B (22). We also evaluated the effect of positioning the “figure 8” decoupling coil perpendicular to the plane of the surface coils (Fig.2D) to minimize distortion of the B_1 field. Table 1 summarizes data for the 5 different configurations including their size, the coupling coefficient k_0, the resonant frequency, and the Q-factor. Figs.5A through 5D show axial maps of the amplitude of the combined simultaneous B_1^+ for five slices separated by 10 mm located near the surface coil center. The maps were obtained using 2-coil arrays with conventional non resonant inductive decoupling (Fig 5A) and three different sizes (Figs 5B–D) of “flat” RIDs (Fig.2A) and an optimized RID (Fig. 5E) described below. In an attempt to minimize the distortion of the B_1 field by the “flat” RID circuit we started with a small coil of 16 mm in diameter (Fig. 5B). As seen from Table 1 the value of f_0 was only 5 MHz less than f_L (ξ=0.017). Despite the small size of the RID coil the B_1 profile of the array was significantly altered at the surface of the sample. To minimize the RF field distortions by increasing ξ while keeping the same RID geometry we increased the RID coil diameter to 22 mm and 28 mm, resulting in in ξ=0.03 (f_0 = 289 MHz) and ξ=0.06 (f_0 = 280 MHz), respectively. However, this caused similar distortions in the B_1 field (Figs. 5C and D). All other types of RIDs presented in Table 1 also produced substantial B_1 field distortion.

To minimize the B_1 field distortion by localizing the RID RF field and at the same time to keep sufficiently large k_0 and ξ we constructed optimized RID circuits (Fig.6). The B_1 map (Fig 5E) obtained using the 2-coil array with the optimized RID demonstrates minimal distortion and is very similar to that obtained using the array with non-resonant inductive decoupling. The optimized RID circuit consisted of two small two-turn inductors connected in series with the surface coils and an electrically insulated resonant coil with a pair of two-turn loops coupled to each surface coil (Fig.6, Table 2). To match Eq. [2], (i.e. the magnetic fluxes generated by adjacent surface coils produce voltages of opposite sign in the RID loops), all four two-turn loops of the RID circuit should be wound in appropriate directions, i.e. two of the four loops were wound clockwise and two of them counterclockwise (Fig.6). In spite of much smaller size of the optimized RID circuits we obtained substantially larger k_0 values (Table 2) as compared to non-optimized RIDs (Table 1).

Figure 7 shows dependence of the loaded Q-factor, Q_L, measured for the 2-coil array decoupled using non resonant inductive decoupling, optimized RID, and the 16 mm “flat” RID (Fig.2A) on distance between the phantom and the surface coils. As seen from the figure presence of the not optimized small RID substantially increases Q_L at distances up to 7 cm, which is much greater the size of the RID circuit itself.

For the 1×16 array using optimized RID (Fig.6) in combination with overlapping we obtained decoupling better than −24 dB for all adjacent coils. Decoupling of −19 dB or better was obtained for all other surface coils. Figure 8A shows axial B_1^+ maps for individual surface coil elements demonstrating good decoupling. Figures 8B and C show combined axial image and corresponding B_1^+ map obtained using the 16-coil (1×16) overlapped array. Homogeneity was evaluated as the standard deviation of the B_1^+ over the entire slice and measured 9.2 %.

DISCUSSION

In the presence of lossy human tissue the mutual impedance Z_{12} may include both reactive and resistive components. For example, in the case of overlapping surface coils, which is one of the most common inductive decoupling techniques, the resistive component can reach substantial values (15,18). Conventional capacitive and inductive decoupling methods only compensate for the reactive component of the Z_{12}, and thus do not provide sufficient decoupling of the elements within an array of overlapped of coils. For example, for an overlapped 1×16 array when unloaded, critically overlapped surface coils were well decoupled to the level below −20 dB. However, when loaded with a human head the best decoupling achieved between adjacent surface coils was ~ −11 dB, which corresponds to $R_{12}/R \sim 0.3$. According to Eq.4 the ratio of the RID-induced reactance to resistance (i.e. imaginary to real changes in the off diagonal elements) is approximately equal to $2Q_0\xi$. For Q_0 of ~200 and the ξ value of ~0.07 ($\Delta f \sim$ 20 MHz) we obtain the value of ~ 30. Since the induced reactance is equal to the mutual inductance between the surface coils, the RID-induced resistance is $\omega kL/2Q_0\xi$. For critically overlapped surface coils (~13.5 mm in our case) the mutual inductance (or k) is close to zero, therefore, the resistive component R_{12}, remains, limiting decoupling to −11dB. Since the RID induces both a reactive and resistive component we induced a small inductive component by reducing the overlap by ~1.5 mm to 12 mm, generating k in the range from 0.02 to 0.025 (mutual inductance M ~ 3 to 4 nH). Using the RID shown in Fig.6 we were then able to compensate (−24 dB coupling) for both the resistive and the reactive (induced by changing overlap) components of the Z_{12} while minimizing B_1 distortion. For the non-adjacent (Δn=2) surface coils where resistive coupling is negligible we used non-resonant inductive decoupling. The Q_U value of individual surface coils was 270 in comparison to 360 for a single surface coil of the same size. Despite some

reduction in Q_U, we obtained a Q_U/Q_L ratio of 2.7 or greater for all coils with the head; including the less loaded anterior surface coils.

Previously we demonstrated, that multiple-channel single-row (1×8) and the double-row (2×8) 7T transceiver phased arrays could be successfully constructed using non-resonant inductive decoupling circuits, consisting of two small, strongly coupled loops each connected in series with the adjacent surface coils (4,9). The decoupling was adjusted mechanically by changing the position of the loops in respect to each other. Mutual inductance strongly depends on surface coil loading determined by the coil-to-sample separation. Since the decoupling is not adjusted on a patient by patient basis, it is crucial to maintain similar loading, e.g. by maintaining a similar distance from each coil to the sample. Proper loading must be also maintained to optimize the coil efficiency and the SNR. The substantial increase in the number of decoupling units for multi-row arrays (e.g. 40 in 2×8 array (8–10)) makes even the one-time mechanical adjustment prior to deployment for experimental use cumbersome. Unlike non-resonant decoupling where the physical separation and/or orientation between the inductive loops have to be adjusted, the RID method provides an easy way to perform the initial adjustment of the decoupling by changing the resonant frequency of the circuit (i.e. adjustment of a single variable capacitor).

When using the RID circuits, their geometry and placement is critical in minimizing the perturbation to the B_1 field generated by the individual coils in the array. All attempts to utilize previously described RID geometries (21–23) for decoupling a pair of 7.5 cm × 9 cm surface coils failed. As seen from Fig.5B even a very small 16 mm “flat” RID circuit (21) produces substantial distortions of the B_1 field of the array. Importantly, these distortions are seen at distances much greater than the size of the RID circuit itself. For “flat” RID circuits substantial increase in Q_L (i.e. decrease in loading) in comparison to non-resonant decoupling is observed at distances of up to 7 cm separation between the object and array (Fig.7). When the difference between f_0 and f_L, Δf, becomes too small even small resonant circuits can produce substantial distortion in the B_1 field of the array. To increase the Δf value the coupling between the RID and the surface coils, k_0 must be increased. Without substantially modifying the RID geometry k_0 can only be increased by increasing the size of the RID loops. Since larger RID loops extend the spatial extent of the distortion, all attempts to minimize it simply by changing the size of the RID circuit failed (Fig.5). Thus the geometry of the RID circuit plays an important role in enabling the size of the RID circuit to be kept small while keeping k_0 sufficiently large. Using the optimized RID circuits shown in Fig.6 we were able to simultaneously satisfy both these requirements.

CONCLUSIONS

We have developed and experimentally verified a novel inductive decoupling method using RID coil, which compensates for both reactive and resistive components of the mutual impedance between the adjacent surface coils. After optimizing the geometry of the RID circuit the method provides an easy way of adjusting the decoupling by changing the resonance frequency.

Acknowledgments

Grant sponsor: National Institutes of Health

Grant numbers: R01- EB009871;R01- EB011639; R01NS081772

Abbreviations

RID	resonant inductive decoupling
SAR	specific absorption rate
FOV	field of view

References

1. Adriany G, Van de Moortele P-F, Wiesinger F, Moeller S, Strupp JP, Andersen P, Snyder C, Zhang X, Chen W, Pruessmann KP, Boesiger P, Vaughan JT, Uurbil K. Transmit and receive transmission line arrays for 7 Tesla parallel imaging. Magn Reson Med. 2005; 53:434–445. [PubMed: 15678527]
2. Mao W, Smith MB, Collins CM. Exploring the limits of RF shimming for high-field MRI of the human head. Magn Reson Med. 2006; 56(4):918–922. [PubMed: 16958070]
3. Ibrahim TS, Tang L. Insight into RF power requirements and B_1 field homogeneity for human MRI via rigorous FDTD approach. J Magn Reson Imag. 2007; 25(6):1235–1247.
4. Avdievich NI, Pan JW, Baehring JM, Spencer DD, Hetherington HP. Short Echo Spectroscopic Imaging of the Human Brain at 7T Using Transceiver Arrays. Magn Res Med. 2009; 62:17–25.
5. Kozlov, M.; Turner, R. Analysis of RF transmit performance for a multi-row multi-channel MRI loop array at 300 and 400 MHz; Proceedings of the Asia-Pacific Microwave Conference; Melbourne, Australia. 2011; p. 1190-1193.
6. Katscher U, Börnert P, Leussler C, van den Brink JS. Transmit SENSE. Magn Reson Med. 2003; 49:144–50. [PubMed: 12509830]
7. Zhu Y. Parallel excitation with an array of transmit coils. Magn Res Med. 2004; 51:775–784.
8. Zhang Z, Yip CY, Grissom W, Noll DC, Boada FE, Stenger VA. Reduction of transmitter B1 inhomogeneity with transmit SENSE slice-select pulses. Magn Reson Med. 2007; 57(5):842–847. [PubMed: 17457863]
9. Avdievich NI. Transceiver phased arrays for human brain studies at 7T. Appl Magn Reson. 2011; 41(2):483–506. [PubMed: 23516332]
10. Gilbert KM, Belliveau J-G, Curtis AT, Gati JS, Klassen LM, Menon RS. A conformal transceive array for 7 T neuroimaging. Magn Reson Med. 2012; 67:1487–1496. [PubMed: 22190335]
11. Shajan, G.; Hoffmann, J.; Scheffler, K.; Pohmann, R. 16-Element dual-row transmitca for 3D RF shimming at 9.4 T; Proceedings of the 20th Annual Meeting ISMRM; Melbourne, Australia. 2012; p. 308
12. Adriany G, Auerbach EJ, Snyder CJ, Gözübüyük A, Moeller S, Ritter J, Van de Moortele PF, Vaughan T, Uğurbil K. A 32-channel lattice transmission line array for parallel transmit and receive MRI at 7 Tesla. Magn Reson Med. 2010; 63(6):1478–1485. [PubMed: 20512850]
13. Wu B, Wang C, Kelley DAC, Xu D, Vigneron DB, Nelson SJ, Zhang X. Shielded microstrip array for 7T human MR imaging. IEEE Trans Med Imag. 2010; 29:179–184.
14. Tropp J. Mutual Inductance in the Bird-Cage Resonator. J Magn Reson. 1997; 126:9–17. [PubMed: 9252272]
15. Roemer PB, Edelstein WA, Hayes CE, Souza SP, Mueller OM. The NMR phased array. Magn Reson Med. 1990; 16:192–225. [PubMed: 2266841]
16. Kraff O, Bitz AK, Kruszona S, Orzada S, Schaefer LC, Theysohn JM, Maderwald S, Ladd ME, Quick HH. An eight-channel phased array RF coil for spine MR imaging at 7 T. Invest Radiol. 2009; 44(11):734–740. [PubMed: 19809342]
17. Keil B, Alagappan V, Mareyam A, McNab JA, Fujimoto K, Tountcheva V, Triantafyllou C, Dilks DD, Kanwisher N, Lin W, Grant PE, Wald LL. Size-optimized 32-channel brain arrays for 3 T pediatric imaging. Magn Reson Med. 2011; 66:1777–1787. [PubMed: 21656548]
18. Wright SM. Full-wave analysis of planar radiofrequency coils and coil arrays with assumed current distribution. Conc Magn Reson B: Magn Reson Eng. 2002; 15(1):2–14.

19. von Morze C, Tropp J, Banerjee S, Xu D, Karpodinis K, Carvajal L, Hess CP, Mukherjee P, Majumdar S, Vigneron DB. An eight-channel, nonoverlapping phased array coil with capacitive decoupling for parallel MRI at 3 T. Conc Magn Reson B: Magn Reson Eng. 2007; 31:37–43.

20. Avdievich, NI.; Pan, JW.; Hetherington, HP. Novel inductive decoupling for single- and double-tuned transceiver phased arrays to compensate for both reactive and resistive components of the mutual impedance; Proceedings of the 20th Annual Meeting ISMRM; Melbourne, Australia. 2012; p. 2806

21. Aal-Braij, R.; Peter, A.; Del Tin, L.; Korvink, JG. A novel inter-resonant coil decoupling technique for parallel imaging; Proceedings of the 17th Annual Meeting ISMRM; Honolulu, USA. 2009; p. 2974

22. Soutome, Y.; Otake, Y.; Bito, Y. Vertical Loop Decoupling Method for Gapped Phased-Array Coils; Proceedings of the 19th Annual Meeting ISMRM; Montreal, Canada. 2011; p. 1859

23. Li Y, Xie Z, Pang Y, Vigneron D, Zhang X. ICE decoupling technique for RF coil array designs. Med Phys. 2011; 38(7):4086–4093. [PubMed: 21859008]

24. Harpen MD. Radiative losses of a birdcage resonator. Magn Reson Med. 1993; 29(5):713–716. [PubMed: 8505911]

25. Pan JW, Twieg DB, Hetherington HP. Quantitative spectroscopic imaging of the human brain. Magn Reson Med. 1998; 40:363–369. [PubMed: 9727938]

26. Beck BL, Jenkins KA, Rocca JR, Fitzsimmons JR. Tissue-equivalent phantoms for high frequencies. Conc Magn Reson B: Magn Reson Eng. 2004; 20B(1):30–33.

27. Picard L, Blackledge M, Decorps M. Improvements in electronic decoupling of transmitter and receiver coils. J Magn Reson B. 1995; 106:110–115.

28. Sucher, M.; Fox, J., editors. Handbook of microwave measurements. New York, London: Willey & Sons, Polytechnic Press of the Polytechnic Institute of Brooklyn; 1963.

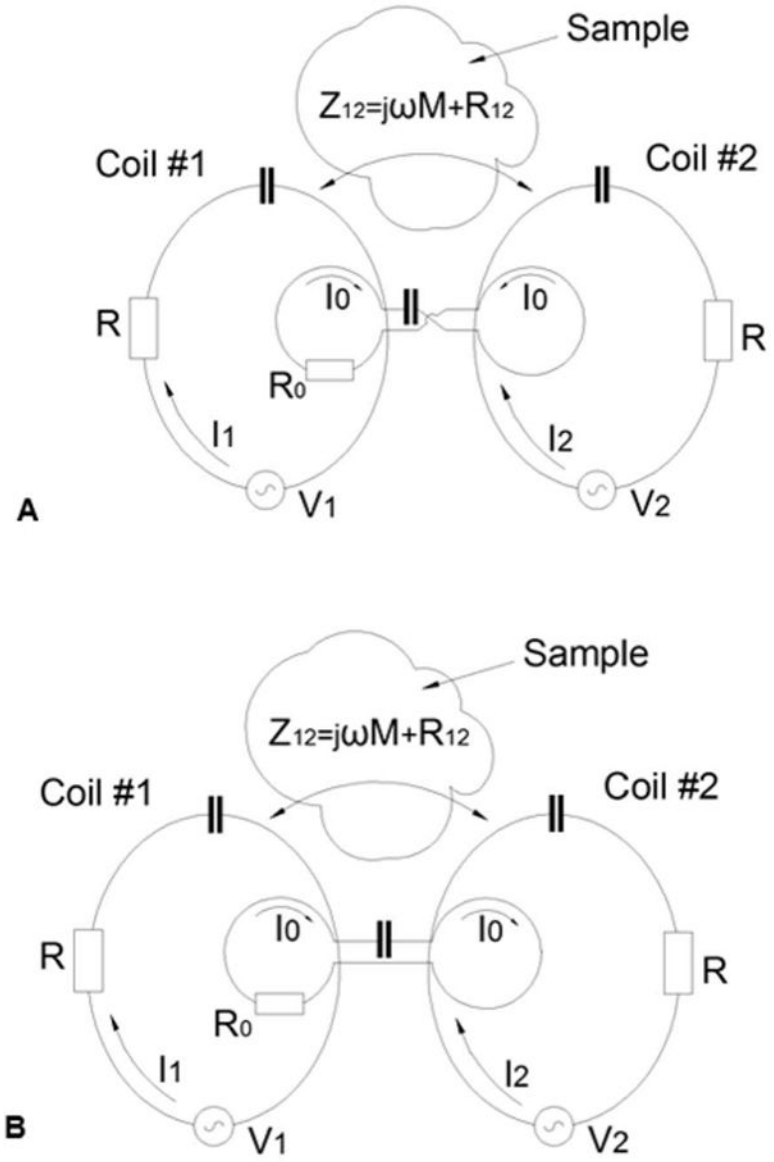

Figure 1.

Schematics demonstrating the general ideas of constructing RID circuits using a “butterfly” (“figure eight”) coil (A) a regular surface coil (B). Two geometrically identical resonant coils #1 and #2 are coupled with their shared impedance Z_{12} and characterized by the inductance L, and the resistance R, In the presence of the sample the mutual impedance Z_{12} contains both reactive, $j\omega M$, and resistive component, R_{12}. RID circuits shown in A) and B) are characterized by the inductance L_0 and the resistance R_0.

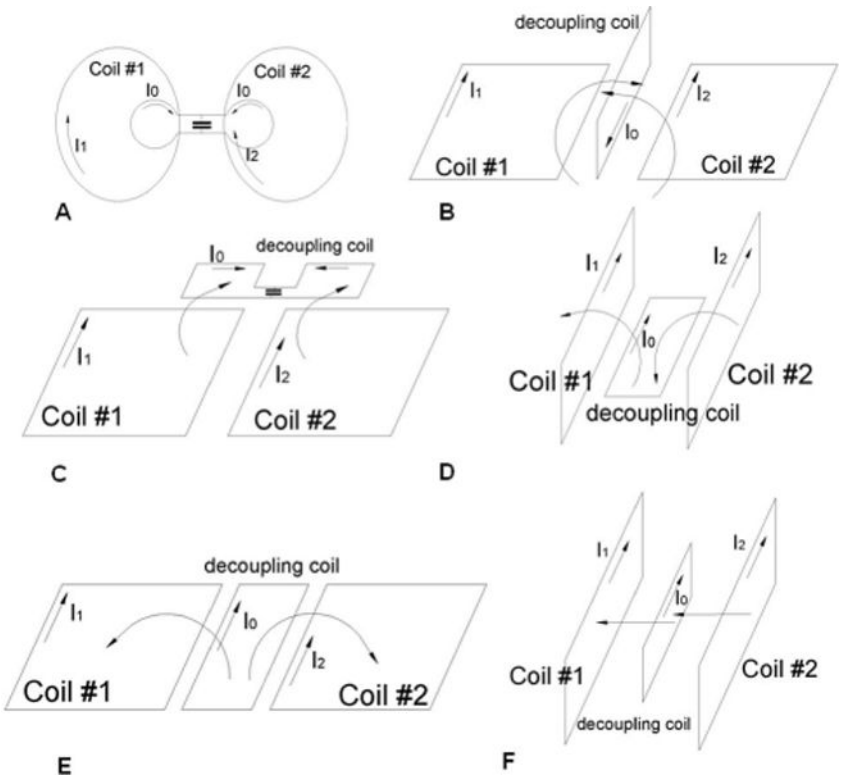

Figure 2.
Schematic of various RID circuits.

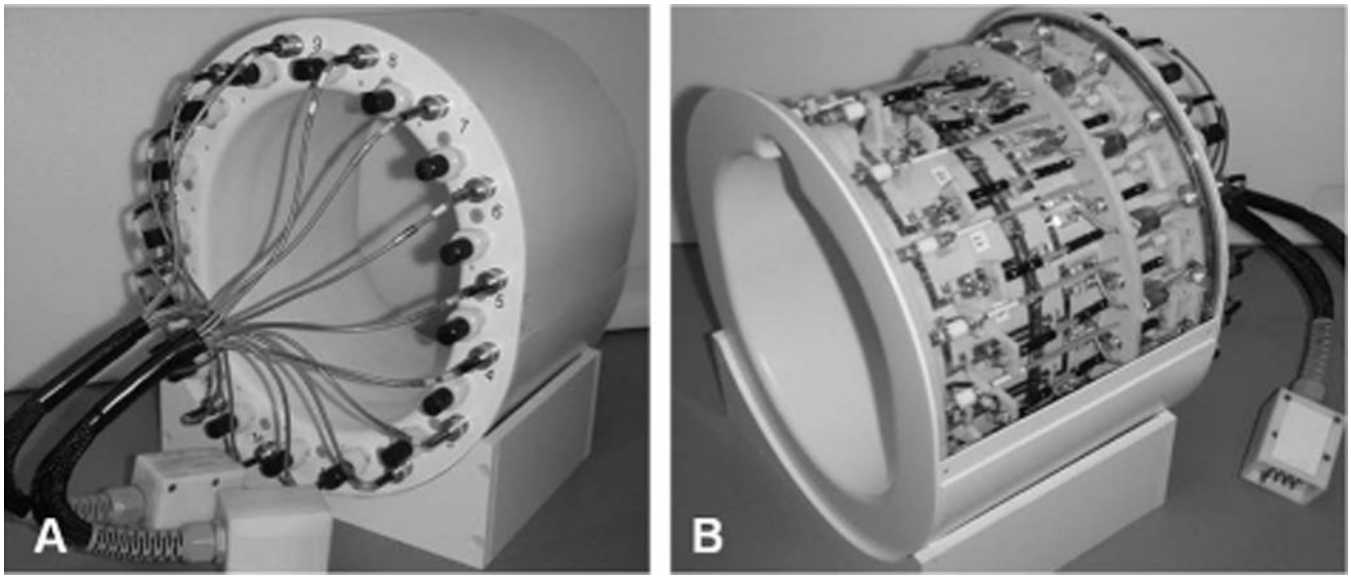

Figure 3.
Photographs of the back (A) and the front (B) sides of the 1×16 phased array. Photo on Fig. 3B shown with the top cover removed.

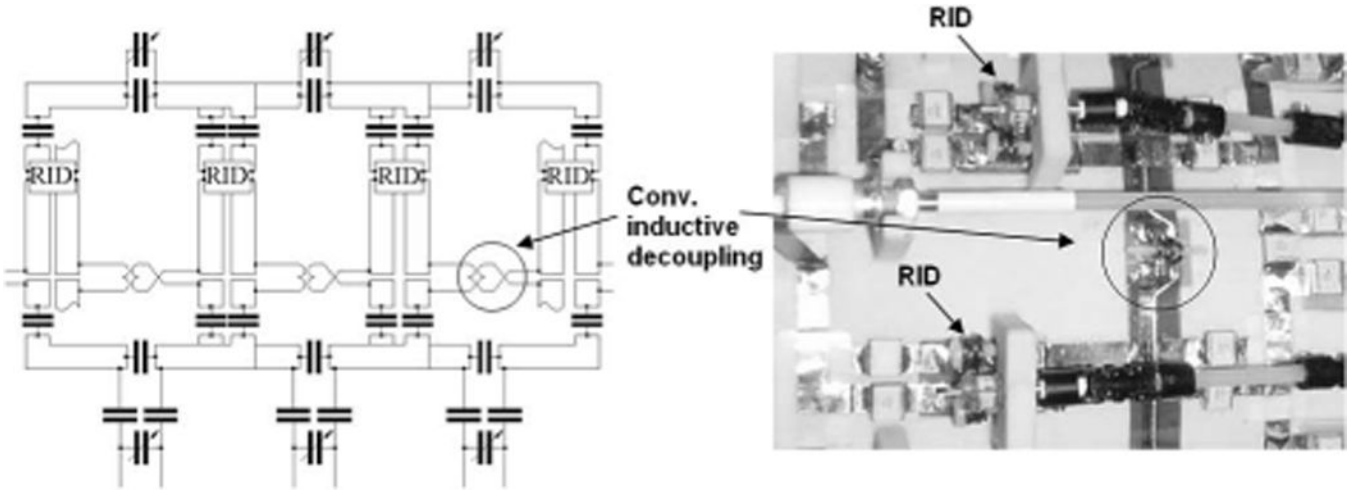

Figure 4.
Schematics of the individual surface coils including matching and decoupling networks.

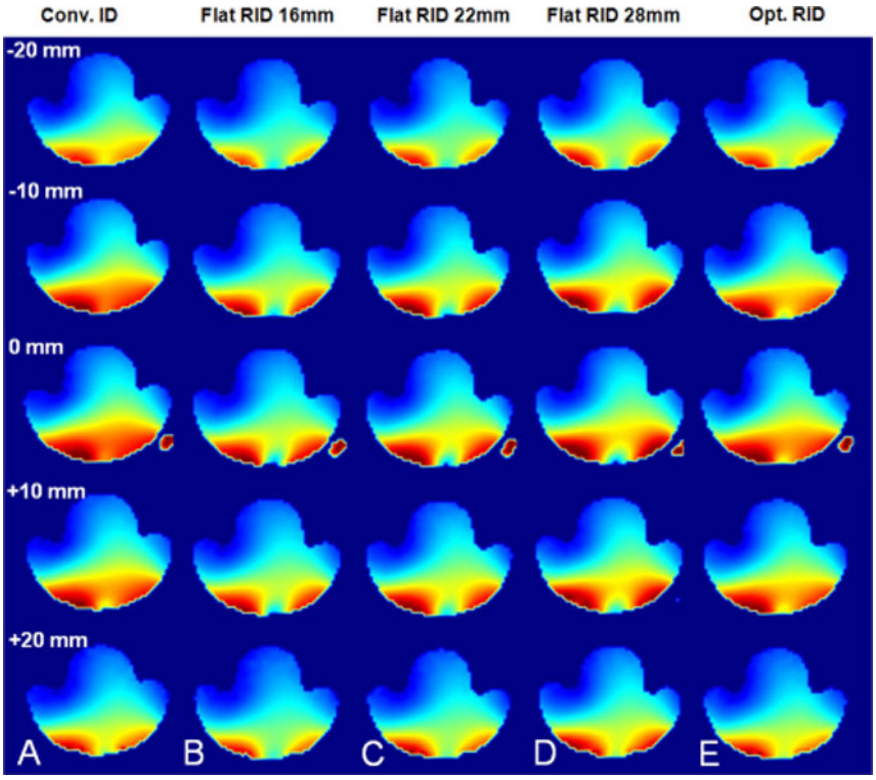

Figure 5.
Axial maps of the amplitude of the combined simultaneous B_1^+ for five slices separated by 10 mm located near the surface coil center. The maps were obtained using 2-coil arrays with conventional non resonant inductive decoupling (A), three different sizes (B–D) of “flat” RIDs (Fig.2A), and the optimized RID (E).

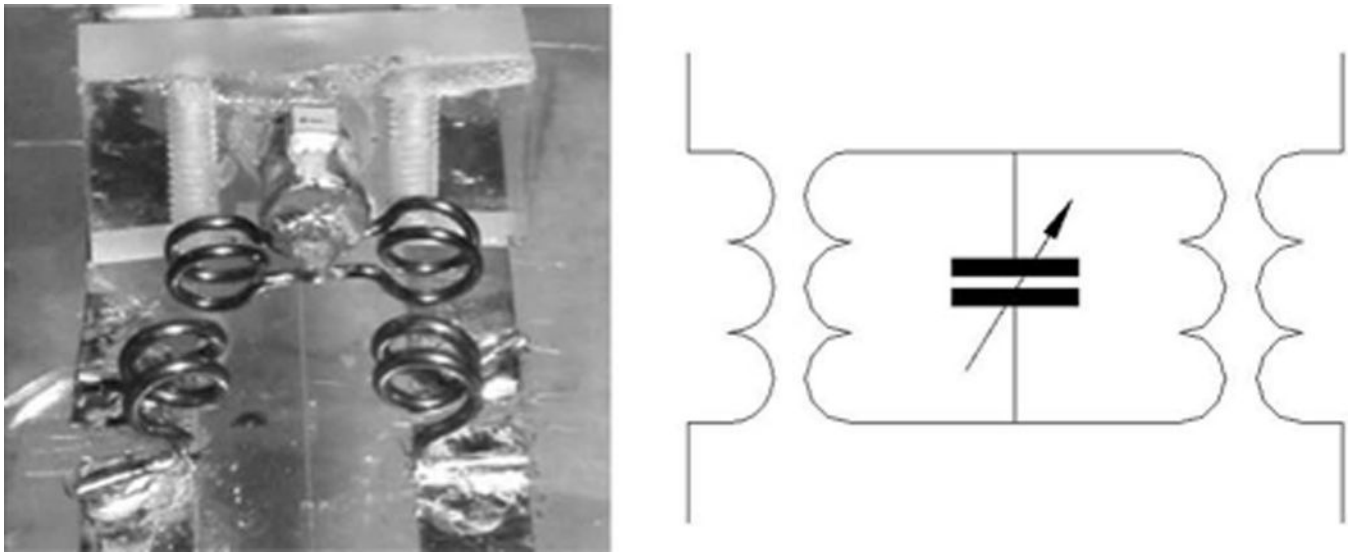

Figure 6.
Photograph and schematic of the optimized RID circuit.

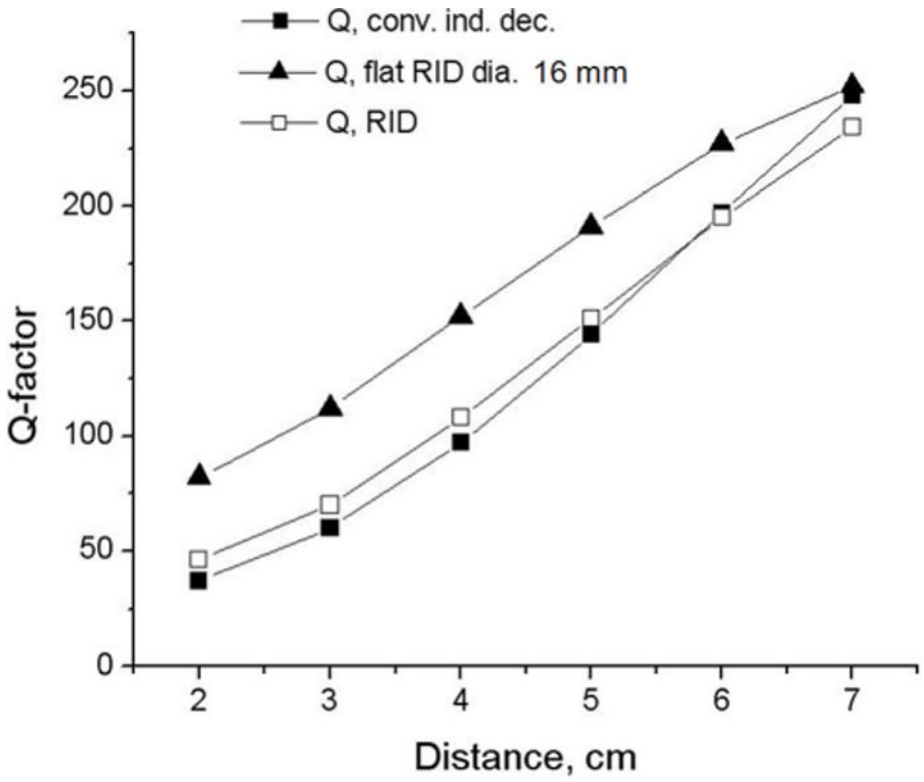

Figure 7.
Dependence of the loaded Q-factor, Q_L, measured for the 2-coil array decoupled using non resonant inductive decoupling, optimized RID, and the 16 mm "flat" RID (Fig.2A) on distance between the phantom and the surface coils.

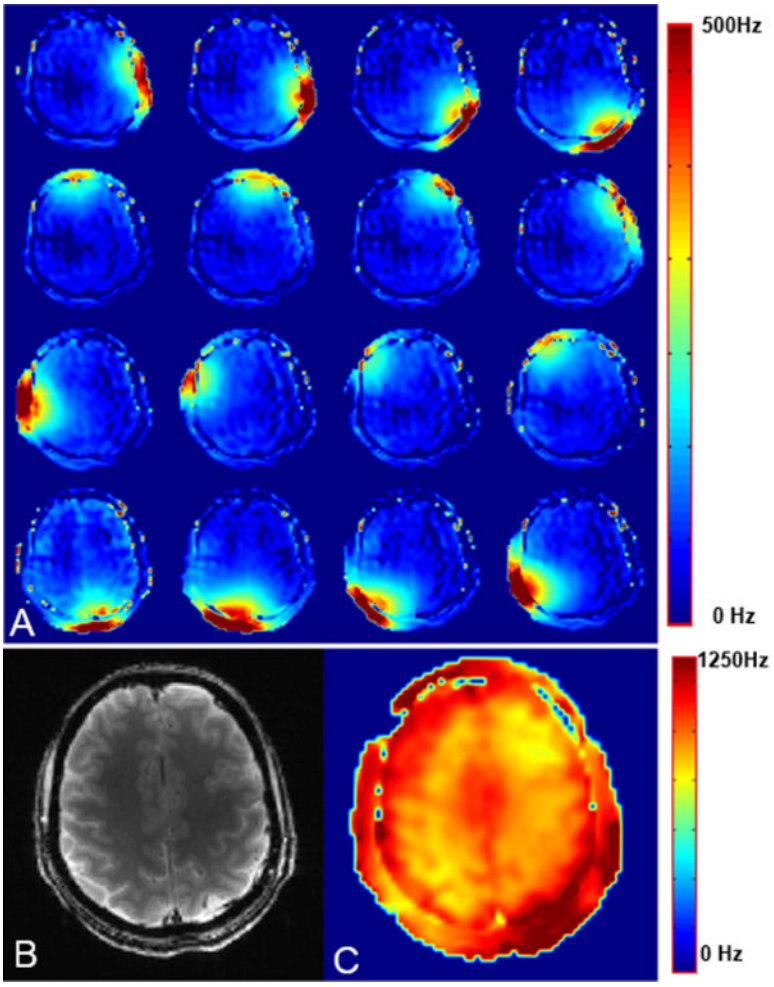

Figure 8.
A) Axial B_1^+ maps for individual surface coil elements. Axial image (B) and corresponding B_1^+ map (C) obtained using the 16-coil (1×16) overlapped array.

Table 1

Parameters of RID circuits.

RID	Loop size	k_0	f_0, MHz	ξ	Q_0
Fig.2A	Dia. 16 mm	0.05	293	0.017	280
Fig.2A	Dia. 22 mm	0.06	289	0.03	325
Fig.2A	Dia. 28 mm	0.09	280	0.064	440
Fig.2B	15 × 60 mm	0.06	288	0.034	380
Fig.2C	20 × 20 mm	0.04	294	0.013	400

Table 2

Parameters of the optimized RID circuit.

k_0	Loop size	f_0, MHz	ξ	Q_0
0.14	Dia. 4 mm	259	0.13	300